Available online at www.sciencedirect.com
ScienceDirect
Journal of Solid State Chemistry 181 (2008) 61–66
JOURNAL OF SOLID STATE CHEMISTRY
www.elsevier.com/locate/jssc

Study on the solid solution of $YMn_{1-x}Fe_xO_3$: Structural, magnetic and dielectric properties

S.L. Samal[a], W. Green[b], S.E. Lofland[c], K.V. Ramanujachary[b], D. Das[d], A.K. Ganguli[a,*]

[a]Department of Chemistry, Indian Institute of Technology, Delhi, Hauz Khas, New Delhi 110016, India
[b]Department of Chemistry, Rowan University, Glassboro, NJ 08028, USA
[c]Department of Physics, Rowan University, Glassboro, NJ 08028, USA
[d]UGC-DAE Consortium for Scientific Research, Kolkata 700098, India

Received 14 August 2007; received in revised form 6 October 2007; accepted 30 October 2007
Available online 11 December 2007

Abstract

The solid solution of $YMn_{1-x}Fe_xO_3$ ($x = 0.0$, 0.1, 0.2, 0.3, 0.5, 1.0) was synthesized from the citrate precursor route. The hexagonal crystal structure related to $YMnO_3$ was stable for $x \leqslant 0.3$. Rietveld refinement was carried out on the composition for $x = 0.3$ and was refined to a major hexagonal phase (~97%) with 3% of orthorhombic $Y(Fe/Mn)O_3$ phase. The *a*-axis lattice constant increases and the *c*-axis lattice constant decreases with *x* for $x \leqslant 0.2$. The increase in the *c*-axis lattice constant at $x = 0.3$ could be due to the doping of significant amount of d^5 ion (high spin Fe^{3+} ion) in a trigonal bipyramidal crystal field. The detailed structural, magnetic and dielectric properties are discussed.

Keywords: Multiferroics; Rietveld refinement; Solid solutions; Mössbauer studies

1. Introduction

Multiferroic materials have been the subject of intense study due to their potential applications in information storage process, spintronics, multiple-state memories, magnetoelectric sensors, etc. [1–7]. They are of remarkable importance because of their unique and strong coupling of electric and magnetic properties, giving rise to the simultaneous presence of more than one ferroic property. $YMnO_3$ and the manganites of heavier rare-earths crystallize in the hexagonal space group $P6_3cm$ [8]. The crystal structure of the hexagonal $YMnO_3$ can be described as corner-linked MnO_5 trigonal bipyramids with free apical oxygen ions. In this structure there appears to be a small tilting of the MnO_5 trigonal bipyramids along the *c*-axis.

The origin of the electric dipole moment perpendicular to the basal plane of this hexagonal perovskite has been attributed to the displacement of Y^{3+} ions relative to the oxide layer comprised by the apical oxygen of the MnO_5 bipyramids. The ferroelectric polarization appears near 900 K [9]. The magnetism of $YMnO_3$ arises from Mn^{3+} spins, which order antiferromagnetically in the *a–b* plane of this structure below the Neel temperature T_N of 70 K [10,11]. Fiebig et al. [12] reported direct evidence of linear coupling between electric and magnetic domains in $YMnO_3$ using second harmonic generation. The in-plane dielectric constant sharply decreases by ~7% near T_N, indicating a strong magnetoelectric coupling [10,13]. On the other hand, the dielectric constant along the *c*-axis shows no apparent anomaly at T_N. It is interesting to note that there is no anomaly of dielectric constant along the *c*-axis in spite of the ferroelectric polarization along that axis.

Several attempts have been made to understand the multiferroic properties in this group of oxides [14] and also efforts have been directed towards syntheses of new oxides of $RMnO_3$ structure [15,16]. Several studies on the effect of doping in yttrium-based manganites have been reported [17–20]. However, most of these studies focused on the doping at the yttrium site, and relatively few studies have been reported on the effect of doping at the Mn site.

*Corresponding author. Fax: +91 11 26854715.
E-mail address: ashok@chemistry.iitd.ernet.in (A.K. Ganguli).

0022-4596/$ - see front matter © 2007 Elsevier Inc. All rights reserved.
doi:10.1016/j.jssc.2007.10.032

Substitution of approximately 22 at% of Ca in the A site of $YMnO_3$ results in a structural phase transition from the hexagonal to the well-known $CaMnO_3$ structure [18]. A similar type of phase transition was also observed when the Mn site was substituted by small divalent cations, Cu^{2+}, Ni^{2+}, and Co^{2+} [21]. Several authors have reported detailed structural, magnetic and dielectric studies on the $YMn_{1-x}TixO_3$ system [22–24]. It appears that the degree of substitution required for structural phase transition does not only depend on the size of the ions. Clearly electronic factors may play a role.

There is only one cursory report in the literature on the substitution of Fe at the Mn site [25]. Veres et al. studied the $YMn_{1-x}Fe_xO_3$ system and reported the formation of pure hexagonal phase up to $x = 0.1$. We have been able to extend the solubility limit to $x = 0.3$ by gel-pyrolysis technique. Here we report the detailed structural, magnetic and dielectric properties of $YMn_{1-x}Fe_xO_3$ system.

2. Experimental

Synthesis of the compounds of the type $YMn_{1-x}Fe_xO_3$ ($0.0 \leqslant x \leqslant 1.0$) was carried out by a low-temperature citrate-gel-precursor route. Stoichiometric amounts of aqueous metal nitrates were prepared by dissolving $MnCO_3$ (CDH, 99.9%), Fe metal (CDH, 99.9%), and Y_2O_3 (Aldrich, 99.99%) powders in a minimum amount of concentrated nitric acid. Y_2O_3 was preheated at 900 °C. The total metal ion concentration was kept at around 0.1 M by adding deionized water. The resulting solution was gently heated to 90 °C and kept at this temperature for 2 h. An appropriate amount of citric acid was added to this solution and refluxed for 6 h at 90 °C under constant stirring. The molar ratio of total metal ion to citric acid was kept at a ratio of 1:2. The solution was then slowly evaporated to form a viscous liquid (reddish brown in color). Further drying was carried out at 120 °C in an oven for 6 h. The precursor powder (grayish brown) was then ground and heated at 500 °C for 5 h in air. The powders obtained at this stage were found to be amorphous by X-ray diffraction studies. All the powders were calcined at 900 °C for 15 h in air which enabled the formation of the desired oxides. The resulting powder was ground and pressed into disks of 8 mm diameter and ~1 mm thickness under a pressure of 1.5 GPa. The disks were sintered in air at 900 °C for 12 h for the dielectric measurements.

All compounds were characterized by a Scintag X-2 powder diffractometer using Cu K_α radiation. X-ray data for Rietveld refinement was collected in the 2θ range of 2–120°. A step size of 0.02° and a step time of 12 s per step were used. Rietveld refinement of X-ray diffraction data of the $YMn_{0.7}Fe_{0.3}O_3$ was carried out using GSAS software [26]. The background was modeled by a shifted Chebyschev polynomial of the first kind with 12 variables and the peak profile was simulated with the pseudo-Voigt function. The refinement involved the cell parameter, scaling factor, 12 terms of background fitting, unit cell and the isotropic thermal parameters for all atoms. The density of the sintered disks was measured by the Archimedes method.

The dielectric properties were measured on disks coated with silver using a HP 4284L LCR meter in the frequency range of 50 Hz to 500 kHz. Temperature variation studies were also carried out in the range of 30–300 °C. The dielectric measurements were carried out repetitively to check the reproducibility of the data. Magnetic data were collected on a Quantum Design, Physical Property Measuring System vibrating sample magnetometer for temperature T between of 5 and 300 K. Data was collected during both the cooling and the warming cycles at an applied magnetic field of 0.5 T. Mossbauer measurements were carried out at room temperature using a 512-channel Mossbauer spectrometer operating in constant acceleration mode. A 10 mCi ^{57}Co in Rh matrix was used as the radioactive source. The spectrometer was calibrated using a 12-μm thick natural iron foil of high purity. The spectra were analyzed with a least-squares fitting program assuming Lorentzian line-shapes.

3. Results and discussion

Single-phase compositions with formula $YMn_{1-x}Fe_xO_3$ with $x \leqslant 0.3$ are observed when the heat treatments were carried out at 900 °C. All the reflections could be satisfactorily indexed on a hexagonal phase (Fig. 1). For $x = 0.5$ composition, ~40% of orthorhombic $YFeO_3$ phase was observed along with the major hexagonal phase of $YMnO_3$. At temperature above 1000 °C, there was evidence of formation of impurities regardless of the value of x. For $x > 0.3$, there were two phases, namely the hexagonal phase related to $YMnO_3$ and an orthorhombic phase related to $YFeO_3$. The relative amount of the orthorhombic to hexagonal phase was observed to increase with increase in x. All samples were black in color and

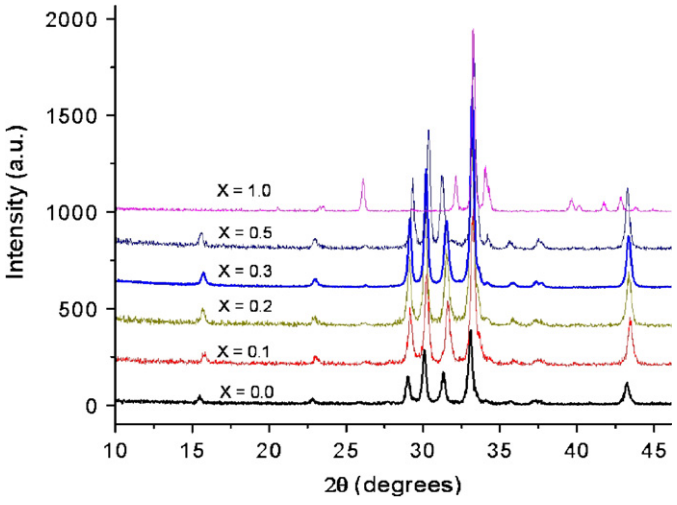

Fig. 1. Powder X-ray diffraction patterns of composition of $YMn_{1-x}Fe_xO_3$ ($0 \leqslant x \leqslant 1.0$).

highly resistive. The density of the sintered pellets was found to be in the range of 87–91% age.

Rietveld refinement studies of the X-ray data was carried out for the composition $x = 0.3$ to verify the phase purity and to estimate the relative fractions of hexagonal and orthorhombic phases. In the X-ray diffraction pattern we observe a few weak shoulders near the $YMnO_3$ phase which complicates the refinement. Hence a very careful refinement was carried out by considering both $YMnO_3$ and $YFeO_3$ phases. A satisfactory model was obtained when 3% of orthorhombic $YFeO_3$ phase along with 97% of the hexagonal $Y(Mn/Fe)O_3$ phase was considered (Fig. 2). The refined position parameters and the thermal parameters are given in Table 1. The refinement converged to R_p and wR_p values of 6.75 and 9.21, respectively. We fixed the occupancies of iron and manganese same as the loaded composition because the refinement of the occupancies of Fe and Mn from the X-ray data is not so accurate due to very less electron density difference between Fe and Mn.

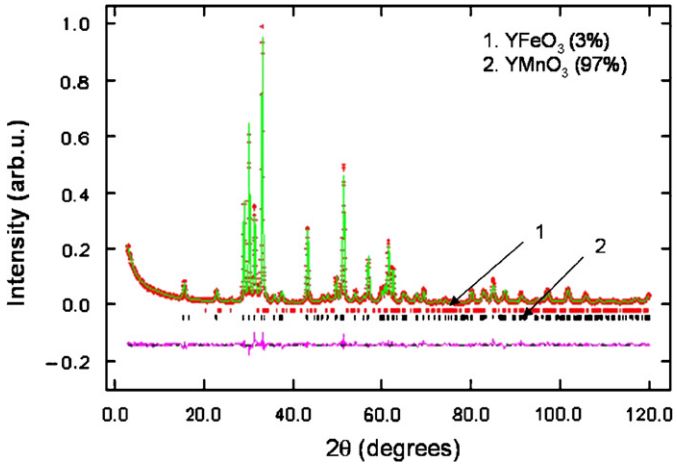

Fig. 2. Final Rietveld plots showing the observed, calculated, and the difference pattern for $YMn_{0.7}Fe_{0.3}O_3$.

The variation of lattice parameters with iron concentration is presented in Fig. 3. We observed that the a-axis lattice parameter increased up to $x \sim 0.2$. On the other hand, the c-axis lattice parameter decreased up to $x = 0.2$ and then increased. The observed trends in the a- and c-axis lattice parameters appear to be similar to those reported for $YMn_{1-x}Ti_xO_3$ up to $x = 0.2$. The observed decrease in c-axis lattice constant up to $x \leqslant 0.2$ may be correlated to the reduced tilting of the MnO_5 bipyramids brought on by the substitution [17]. The increase of a-axis cell parameter in the $YMn_{1-x}Ti_xO_3$ has been attributed to the variation in the sizes of Mn^{3+} and Ti^{4+} ions. However, the increase in the a-axis cell parameter in our system is difficult to explain in view of the similar sizes of Mn^{3+} and Fe^{3+} ions (0.58 Å in fivefold coordination).

In an attempt to explain the increase in the c-axis lattice parameter in $YMn_{1-x}Fe_xO_3$ for $x > 0.2$, we considered electronic effects. Gopalakrishnan et al. [27], in their study on $La_{2-x}Sr_xNiO_4$, have reported that the intra d-band transitions may be the cause of the lattice-parameter anomalies. The same explanation would not apply to our system since the Mn^{3+} and Fe^{3+} are in a trigonal bipyramidal (TBP) geometry and the crystal field effects on the d-orbital electron are different than those in an

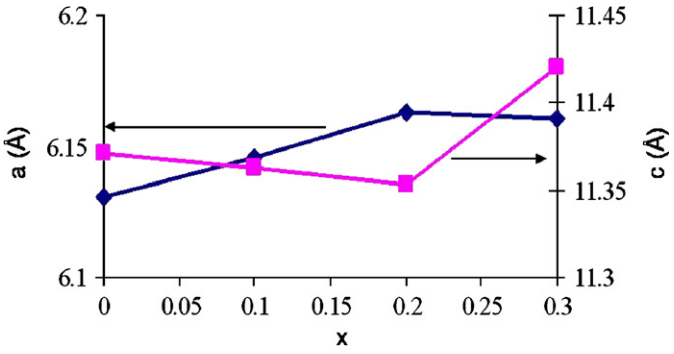

Fig. 3. The variation of a- and c-axis lattice parameters as a function of x.

Table 1
Rietveld refinement data of $YMn_{0.7}Fe_{0.3}O_3$

Atom	Wyckoff symbol	Coordinates			Fractional occupancy	$U_{iso} \times 100$
		x	y	z		
Y(1)	4*b*	1/3	2/3	0.2694(2)	1.0	1.05(4)
Y(2)	2*a*	0	0	0.2336(2)	1.0	0.74(6)
Mn	6*c*	0.3348(9)	0	0.0106(5)	0.7	1.62(4)
Fe	6*c*	0.3348(9)	0	0.0106(5)	0.3	1.62(4)
O(1)	6*c*	0.3427(12)	0	0.1778(5)	1.0	2.58
O(2)	6*c*	0.6941(13)	0	0.3468(6)	1.0	2.80
O(3)	4*b*	0	0	0.0243(7)	1.0	3.31(16)
O(4)	2*a*	1/3	2/3	0.4898(8)	1.0	2.87(15)

Lattice parameter.
$YMnO_3$ $a = 6.1708(1)$ Å, $c = 11.4204(2)$ Å.
$YFeO_3$ $a = 5.5673(7)$ Å, $b = 7.4985(8)$ Å, $c = 5.2656(6)$ Å.
$R_p = 6.75$, $wR_p = 9.21$, $\chi^2 = 2.99$.
Phase %age = 97% $YMnO_3$ and 3% $YFeO_3$.

octahedral crystal field. In $YMn_{1-x}Fe_xO_3$ both the Fe and Mn are trivalent. Assuming the high spin configuration, the occupancy of the electrons in d-orbitals in $Fe^{3+}(d^5)$ and $Mn^{3+}(d^4)$ may be shown as given in Fig. 4. Though the effect of tilting of MnO_5 polyhedra on the energy level of d-orbitals cannot be neglected, the given schematic energy level diagram of Mn^{3+} and Fe^{3+} assumes ideal geometry. The extra electron in the trivalent Fe enters to d_{z^2} orbital in TBP crystal-field geometry. With doping more Fe in the Mn site, the population of d_{z^2} electron increases, which could be the reason for the elongation of c axis in this system.

Mössbauer study was carried out to confirm the oxidation state of iron. Fig. 5 shows the room temperature Mössbauer spectra of $YMn_{1-x}Fe_xO_3$, $0.1 \leqslant x \leqslant 0.3$. The isomer shift values (Table 2) are consistent with trivalent iron with TBP crystal field in these compounds. The large quadrupole splitting (QS) values show significant distortions at the Mn/Fe site in the crystal system. Also there is a small increase in the QS value with the increase of x in the sample, suggesting an increasing local distortion with Fe content.

Figs. 6(a and 6(b) show temperature variation of magnetic susceptibility and inverse magnetic susceptibility of $YMn_{1-x}Fe_xO_3$, respectively. No kink in the magnetic susceptibility, indicative of antiferromagnetic ordering, was seen down to 5 K for any of the samples. This behavior has been observed before in the parent compound [10,13,28], though the magnetic transition was apparent in the specific heat measurement [10]. The Weiss temperature and magnetic moment (Table 3) were calculated from the

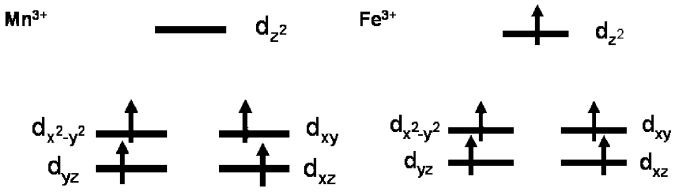

Fig. 4. The electronic configuration of high spin Mn^{3+} and Fe^{3+} ions in trigonal bipyramidal geometry.

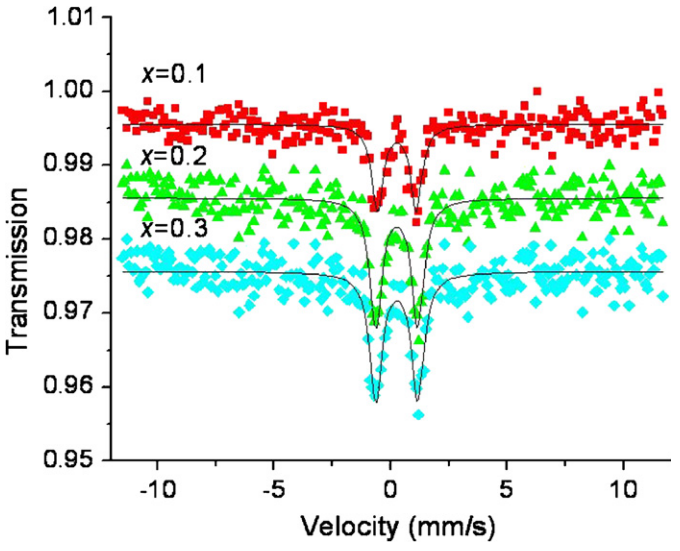

Fig. 5. Mossbauer spectra of $YMn_{1-x}Fe_xO_3$ for (a) $x = 0.1$, (b) $x = 0.2$, and (c) $x = 0.3$.

Table 2
Mossbauer parameters for $YMn_{1-x}Fe_xO_3$

X	Isomer shift (mm/s)	Quadrupole splitting (mm/s)	Full-width half-maximum (mm/s)
0.1	0.26	0.83	0.58
0.2	0.26	0.89	0.65
0.3	0.27	0.92	0.57

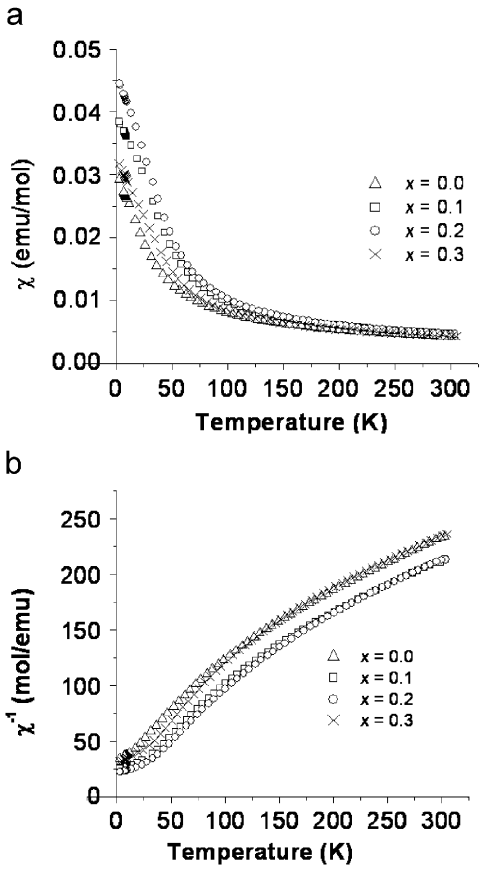

Fig. 6. Temperature dependence of (a) molar magnetic susceptibility (χ) and (b) inverse molar magnetic susceptibility of $YMn_{1-x}Fe_xO_3$, $x = 0.0$, 0.1, 0.2, and 0.3 at an applied field of 5 kOe.

Table 3
Curie–Weiss analysis of the susceptibility of $YMn_{1-x}Fe_xO_3$

X	Weiss temperature (K)	Experimental magnetic moment (μ_B)	Theoretical magnetic moment (μ_B)
0	−169	3.99	4.89
0.1	−154	4.12	5.01
0.2	−175	4.07	5.12
0.3	−208	4.16	5.23

linear part of the high-temperature inverse susceptibility data ($T > 200$ K, above the Weiss temperature). The theoretical magnetic moments were calculated by assuming both Mn and Fe in trivalent state. The experimental data reasonably match with the theoretical values although somewhat lower in all cases. The Weiss temperature, a measure of the interaction strength, has a minimum at $x = 0.1$. Perhaps the substitution of Fe into the Mn site dilutes the Mn network; however with increasing Fe, there are more Fe–Fe nearest neighbors ($\sim 4\times$), leading to a larger average interaction. That is the Fe–Fe interaction is the strongest and the Mn–Fe is the weakest. Presumably, there should be some concomitant magnetic frustration, which could be found from the ordering temperature, which requires either neutron diffraction or heat capacity studies.

The temperature dependence of the dielectric constant and the dielectric loss of the oxygen annealed compounds are shown in Figs. 7(a and b), respectively (100 kHz). It is well known that the dielectric constant and the ferroelectric transition temperature depend on the grain size and density of the material [29]. The dielectric constant decreases, as expected, with decrease in density. So we corrected the dielectric constant values by taking into consideration the porosity of the material using the equation $\varepsilon_{Theo} = \varepsilon_{Meas}(2/2 - 3P)$, where ε_{Theo}, ε_{Meas}, and P are the theoretical dielectric constant, the measured dielectric constant and porosity, respectively. The dielectric constant ε and the dielectric loss $\tan\delta$ both remain constant up to 250 °C. A rapid rise in the dielectric constant as well as dielectric loss above 250 °C for all the compositions is clearly evident and consistent with a ferroelectric ordering temperature above 300 °C, reported previously [30]. Note that the dielectric properties of as-synthesized compounds showed a smaller dielectric constant value than that of the oxygen-annealed compounds. Hence the oxygen annealing on these compounds is necessary to get better dielectric properties.

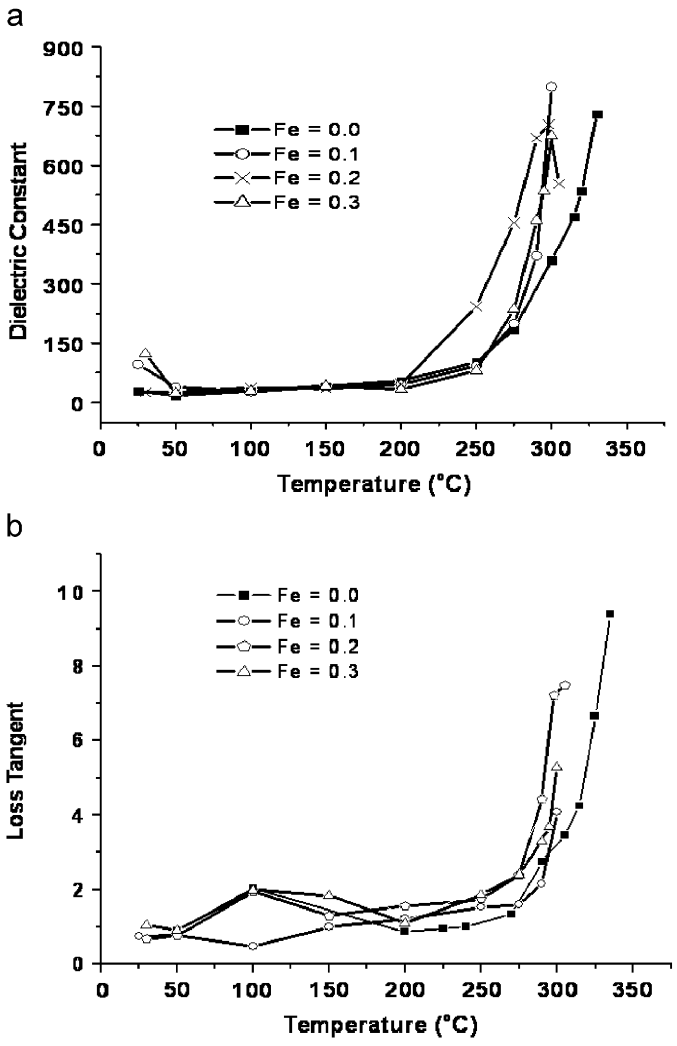

Fig. 7. Temperature dependence of (a) dielectric constant and (b) dielectric loss of $YMn_{1-x}Fe_xO_3$ at 100 kHz.

4. Conclusions

We have stabilized the $YMn_{1-x}Fe_xO_3$ solid solution in hexagonal phase up to $x = 0.3$ synthesized by the citrate precursor route. There is an increase in the c-axis lattice parameter near $x = 0.3$, which may be due to increase in electron population in d_{z^2} orbital. While the magnetic ordering temperature could not be determined from magnetization measurements, the high-temperature susceptibility indicated that the magnetic moments were somewhat smaller than expected and that the Mn–Fe exchange interaction is relatively weak. The dielectric properties show all the compositions have possible ferroelectric behavior above 300 °C.

Acknowledgment

The authors thank Mr. Samrat for the Mossbauer measurement. S.L. Samal would like to thank CSIR for a research fellowship. KVR acknowledges the CP-STIO award from the Department of Science Technology, India.

References

[1] S.V. Kiselev, R.P. Ozerov, G.S. Zhdanov, Sov. Phys. Dokl. 7 (1962) 742–744.
[2] M. Fiebig, J. Phys. D 38 (2005) R123–R152.
[3] W. Prellier, M.P. Singh, P. Murugavel, J. Phys.: Condens. Matter 17 (2005) R803–R832.
[4] C.-W. Nan, Phys. Rev. B 50 (1994) 6082–6088.
[5] J. Wang, J.B. Neaton, H. Zheng, V. Nagarajan, S.B. Ogale, B. Liu, D. Viehland, V. Vaithyanathan, D.G. Schlom, U.V. Waghmare, N.A. Spaldin, K.M. Rabe, M. Wuttig, R. Ramesh, Science 299 (2003) 1719–1722.
[6] X. Qi, J. Dho, R. Tomov, M.G. Blamire, J.L. MacManus-Driscoll, Appl. Phys. Lett. 86 (2005) 062903(1)–062903(3).
[7] C. Ederer, N.A. Spaldin, Phys. Rev. B 71 (2005) 060401(1)–060401(4).
[8] B.B. van Aken, A. Meetsma, T.T.M. Palstra, Acta Crystallogr. Sect. C 57 (2001) 230–232.
[9] T. Lonkai, D.G. Tomuta, U. Amann, J. Ihringer, R.W.A. Hendrikx, D.M. Többens, J.A. Mydosh, Phys. Rev. B 69 (2004) 134108(1)–134108(10).

[10] A. Muñoz, J.A. Alonso, M.J. Martínez-Lope, M.T. Casáis, J.L. Martínez, M.T. Fernández-Daíz, Phys. Rev. B 62 (2000) 9498–9510.
[11] T. Katsufuji, S. Mori, M. Masaki, Y. Moritomo, N. Yamamoto, H. Takagi, Phys. Rev. B 64 (2001) 104419(1)–104419(6).
[12] M. Fiebig, T. Lottermoser, D. Fröhlich, A.V. Goltsev, R.V. Pisarev, Nature (London) 419 (2002) 818–820.
[13] Z.H. Huang, Y. Cao, Y.Y. Sun, Y.Y. Xue, C.W. Chu, Phys. Rev. B 56 (1997) 2623–2626.
[14] B.B. Van Aken, T.T.M. Palstra, A. Filippetti, N.A. Spaldin, Nat. Mater. 3 (2004) 164–170.
[15] S. Malo, A. Maignan, S. Marinel, M. Hervieu, K.R. Poeppelmeier, B. Raveau, Solid State Sci. 7 (2005) 1492–1499.
[16] N. Floros, J.T. Rijssenbeek, A.B. Martinson, K.R. Poeppelmeier, Solid State Sci. 4 (2002) 1495–1498.
[17] T. Katsufuji, M. Masaki, A. Machida, M. Moritomo, K. Kato, E. Nishibori, M. Takata, M. Sakata, K. Ohoyama, K. Kitazawa, H. Takagi, Phys. Rev. B 66 (2002) 134434(1)–134434(8).
[18] C. Moure, M. Villegas, J.F. Fernandez, J.M. Tartaj, P. Duran, J. Mater. Sci. 34 (1999) 2565–2568.
[19] B.B. van Aken, J.W.G. Bos, R.A. de Groot, T.T.M. Palstra, Phys. Rev. B 63 (2001) 125127(1)–125127(4).
[20] I.H. Ismailzade, G.A. Smolenskii, V.I. Nesterenko, F.A. Agaev, Phys. Status Solidi A 5 (1971) 83–89.
[21] C. Moure, D. Gutierrez, O. Pena, P. Duran, J. Solid State Chem. 163 (2002) 377–384.
[22] Y. Aikawa, T. Katsufuji, T. Arima, K. Kato, Phys. Rev. B 71 (2005) 184418(1)–184418(5).
[23] T. Asaka, K. Nemoto, K. Kimono, T. Arima, Y. Matsui, Phys. Rev. B 71 (2005) 014114(1)–014114(6).
[24] S. Mori, J. Tokunaga, Y. Horibe, Y. Aikawa, T. Katsufuji, Phys. Rev. B 72 (2005) 224434(1)–224434(5).
[25] A. Veres, J.G. Noudem, S. Fourrez, G. Bailleul, Solid State Sci. 8 (2006) 137–141.
[26] A.C. Larson, R.B. Von Dreele, GSAS—General Structure Analysis System, Los Alamos National Laboratory, Los Alamos, NM, 1994.
[27] J. Gopalakrishnan, G. Colsmann, B. Reuter, J. Solid State Chem. 22 (1977) 145–149.
[28] S.A. Kizhaev, V.A. Bokov, O.V. Kachalov, Sov. Phys. Solid State 8 (1966) 215–216.
[29] E.S. Kim, H.S. Park, K.H. Yoon, Mater. Chem. Phys. 79 (2003) 213–217.
[30] F. Bertaut, F. Forrat, P. Fang, C. R. Acad. Sci. 256 (1963) 1958–1961.